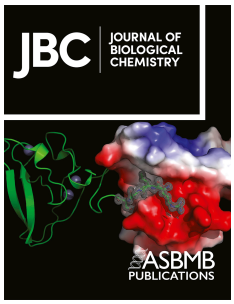

Glucocorticoid receptor Thr524 phosphorylation by MINK1 induces interactions with 14-3-3 protein regulators

Claire C. Munier, Leonardo De Maria, Karl Edman, Anders Gunnarsson, Marianna Longo, Carol MacKintosh, Saleha Patel, Arjan Snijder, Lisa Wissler, Luc Brunsveld, Christian Ottmann, Matthew W.D. Perry

PII: S0021-9258(21)00329-X

DOI: https://doi.org/10.1016/j.jbc.2021.100551

Reference: JBC 100551

To appear in: *Journal of Biological Chemistry*

Received Date: 6 August 2020

Revised Date: 8 March 2021

Accepted Date: 16 March 2021

Please cite this article as: Munier CC, De Maria L, Edman K, Gunnarsson A, Longo M, MacKintosh C, Patel S, Snijder A, Wissler L, Brunsveld L, Ottmann C, Perry MWD, Glucocorticoid receptor Thr524 phosphorylation by MINK1 induces interactions with 14-3-3 protein regulators, *Journal of Biological Chemistry* (2021), doi: https://doi.org/10.1016/j.jbc.2021.100551.

Glucocorticoid receptor Thr524 phosphorylation by MINK1 induces interactions with 14-3-3 protein regulators

Claire C. Munier[1,2], Leonardo De Maria[1], Karl Edman[3], Anders Gunnarsson[3], Marianna Longo[4], Carol MacKintosh[4], Saleha Patel[5], Arjan Snijder[3], Lisa Wissler[3], Luc Brunsveld[2], Christian Ottmann[2], Matthew W. D. Perry[1,*]

[1] Research and Early Development, Respiratory & Immunology, BioPharmaceuticals R&D, AstraZeneca, Gothenburg, Sweden.

[2] Laboratory of Chemical Biology, Department of Biomedical Engineering and Institute for Complex Molecular Systems, Technische Universiteit Eindhoven, Den Dolech 2, 5612 AZ Eindhoven, The Netherlands.

[3] Discovery Sciences, BioPharmaceuticals R&D, AstraZeneca, Gothenburg, Sweden.

[4] Division of Cell and Developmental Biology (C.M.), College of Life Sciences, University of Dundee, Dundee DD1 5EH, Scotland, UK.

[5] Discovery Biology, Discovery Sciences, R&D, AstraZeneca, Cambridge, UK

* Corresponding author: Matthew W. D. Perry

E-mail: Matthew.Perry@astrazeneca.com

Running title: 14-3-3 Regulation of GR by MINK1 phosphorylation

Keywords: 14□3□3 protein, glucocorticoid receptor, MINK1 kinase, nuclear receptor, phosphorylation, protein□protein interaction

Abstract

Glucocorticoid receptor (GR) is a ligand-dependent transcription factor that plays a central role in inflammation. GR activity is also modulated *via* protein–protein interactions, including binding of 14-3-3 proteins induced by GR phosphorylation. However, the specific phosphorylation sites on GR that trigger these interactions and their functional consequences are less clear. Hence, we sought to examine this system in more detail. We used phosphorylated GR peptides, biophysical studies and X-ray crystallography to identify key residues within the ligand binding domain of GR, T524 and S617, whose phosphorylation results in binding of the representative 14-3-3 protein 14-3-3ζ. A kinase screen identified MINK1 as responsible for phosphorylating T524 and ROCK1 for phosphorylating S617; cell-based approaches confirmed the importance of both GR phosphosites and MINK1 but not ROCK1 alone in inducing GR–14-3-3 binding. Together our results provide molecular-level insight into 14-3-3-mediated regulation of GR and highlight both MINK1 and the GR–14-3-3 axis as potential targets for future therapeutic intervention.

Introduction

GR is a ligand dependent transcription factor which belongs to the superfamily of nuclear hormone receptors, a highly conserved ligandable protein family. Ubiquitously expressed throughout the human body, GR regulates the expression of thousands of genes that control a wide range of fundamental processes (1). The role of GR is to mediate the actions of glucocorticoids, steroid hormones produced by the adrenal cortex and under tight regulation by the hypothalamic-pituitary-adrenal axis (2). GR Agonists are widely prescribed drugs used in the treatment of inflammatory and immunological conditions as well as the treatment of some cancers. By their nature in affecting the transcription of many genes, GR agonists are associated with multiple effects, both beneficial and undesired, thus understanding the underlying signaling network of GR is of great importance (2–4).

GR is divided into three major domains: the N-terminal domain (NTD), the DNA binding domain (DBD) and the C-terminal ligand binding domain (LBD) with a short hinge region (HR) between the DBD and LBD. Upon translocation to the nucleus, GR binds to GR binding DNA sequences and, as a scaffolding protein, brings different cofactors and other transcription factors together to build a transcriptional complex that regulates gene expression (1, 5, 6). Additionally, GR can take part in nongenomic signaling (5, 6), adding another layer of complexity, whilst GR turnover is regulated by the ubiquitin-proteasome pathway (7).

14-3-3 proteins form a family of eukaryotic regulatory proteins that act as dimers, principally heterodimers, which recognize and bind to specific pairs of phosphorylated serine/threonine residues, thus forming part of a regulatory system with kinases and phosphatases (8, 9). 14-3-3 proteins are involved in regulating a large number of cellular processes, such as cell cycle progression, apoptosis, intracellular protein trafficking and signal transduction (8). More than 200 structurally and functionally diverse 14-3-3 protein partners have been identified (10). 14-3-3 has been, for example, reported to interact with numerous nuclear hormone receptors to modulate their activity, including estrogen receptor α (ERα) (11), estrogen-related receptor γ (ERRγ) (12) and pregnane X receptor (PXR) (13).

Early evidence for the interaction between 14-3-3 and GR came from yeast two-hybrid studies (14) and immunoaffinity chromatographic studies on rat liver cytosol (15). The 14-3-3 isoform η has been reported to bind the GR LBD and increase GR transcriptional activity through blocking the ubiquitin-proteasome GR degradation pathway (14, 16). The 14-3-3 β and γ isoforms have been found to bind full length GR and to up-regulate GR activity in a ligand dependent manner (17). GR transcriptional activity was, however, repressed by phosphorylation of S134 in a p38 MAPK-dependent manner, driving GR interaction with 14-3-3ζ (18). Interestingly, 14-3-3σ has been reported to bind two different portions of GR: GR S134 or GR LBD and to antagonize GR transcriptional activity (17, 19, 20). The interaction between 14-3-3 and GR has been suspected to play a role in pathological inflammatory disorders (18) and cancer (20).

Given this background we wanted to explore the role of the GR–14-3-3 protein–protein interaction using a bottom-up molecular approach, since information on this level is virtually absent. Identification of the GR residues, whose phosphorylation is recognized by 14-3-3, and the kinases responsible for phosphorylation of these GR sites is crucial to gain this molecular-level insight into the mechanism underlying the 14-3-3 mediated GR regulation. Herein we explore for the first time this molecular mechanism and report on the phosphosites of GR that are recognized by 14-3-3. The GR-14-3-3 interaction was first

investigated at the GR peptide level, then extended to the GR ligand binding domain and finally to full-length proteins in cells to validate the relevance of the peptide studies. We found that T524 of GR is the most important phosphosite, particularly in association with S617. We also found that the kinase MINK1, not previously associated with GR, phosphorylates the key T524 residue and that, in a cellular system, this kinase is required for most of the binding of GR to 14-3-3. This work thus contributes to unravelling the long-standing question on the 14-3-3 regulation of GR signaling pathways, assessing the GR–14-3-3 protein–protein interaction implication in disease state and highlighting both MINK1 and the GR–14-3-3 axis as potential targets for future therapeutic intervention.

Results

14-3-3 Binding to phosphopeptides, centered on putative 14-3-3 binding sites of GR

Although 14-3-3 proteins can recognize some unphosphorylated sequences in non-physiological contexts, such as R18 and exoenzyme S (21, 22), the normal recognition elements in binding with 14-3-3 are phosphoserines and phosphothreonines (9). Potential phosphosites on GR for recognition by 14-3-3 proteins were identified from literature reports and by use of the 14-3-3-Pred webserver (www.compbio.dundee.ac.uk/1433pred) (23) (Fig. **1a**). We synthesized 13-mer peptides centered on each of these residues and measured their affinity to 14-3-3ζ and σ by both fluorescence polarization (FP) and surface plasmon resonance (SPR).

Multiple potential phosphosites on GR have been reported in the literature including T8, S45, S113, S134, S203, S211, S226, S234, S267 and S404 (6, 24). All are part of the NTD and, apart from T8 and S404, they are located within the transactivation domain activation function 1, suggesting a role in the modulation of GR transcriptional activity (6, 24). Surprisingly, only one of these phosphosites, GR S134, was identified as a putative 14-3-3 binding site by the prediction algorithm. The 13-mer peptide centered on GR S134 was the only phosphopeptide, from this set, to show an interaction with 14-3-3 (K_d=90 and 110 μM with 14-3-3ζ and 14-3-3σ respectively) (Fig. **1b**).

Seven putative GR phosphorylation sites were identified by the algorithm as candidates for recognition by 14-3-3 proteins: S83, S134, T493, T524, T561, S617 and T635. Six of these 13-mer GR peptides showed binding with 14-3-3ζ and σ, the exception being pT493. Peptides centered on the GR residues pT524 and pS617 were found to be the strongest binders with K_ds in the low micromolar range (Fig. **1b-f**, Supporting Fig. **S1**). Of note, these two sites belong to the GR LBD.

Interaction of 14-3-3 with a dimeric peptide: GR_pT524-pS617

14-3-3s act as a dimer and thus effectively provide 2 amphipathic binding grooves (8). Many 14-3-3 targets (PKC, C-Raf, CFTR, Gab2) have been shown to interact through tandem phosphosites simultaneously, greatly increasing their binding affinity with 14-3-3 (25–28). Hence, a dimeric peptide, GR_pT524-pS617, consisting of the two 13-mers GR_pT524, GR_pS617 identified above, linked by a pentaglycine moiety to permit flexibility (25), was synthesized and tested for binding to 14-3-3ζ. The dimeric peptide displayed a remarkable avidity effect, with a 1000-fold improvement of its binding affinity with 14-3-3ζ, compared to the individual monomers, and a K_d of 18 nM, one of the highest affinities reported for a 14-3-3 motif (25–28) (Fig. **2** and Supporting Fig. **S1**).

Previous work has reported 14-3-3 to interact with phosphosites from different domains of its partner proteins (29). Hence, the phosphosites from GR NTD and GR LBD could also be envisioned to interact simultaneously with a 14-3-3 dimer. We had identified two potential 14-3-3 binding sites in the NTD: S83 and S134, from the bioinformatic analysis. To test this hypothesis, similar 31-mer peptides containing pentaglycine linked 13-mers, GR_pS83-pT524, GR_pS134-pT524 and GR_pS83-pS134, were synthesized. These peptides also showed significantly increased binding affinity with 14-3-3ζ compared to the monomers, but were least 15-fold weaker than GR_pT524-pS617 (Fig. **2**).

Identification of GR_pT524-pS617 binding hotspots by mutation and alanine scan

We synthesized 24 peptides where each amino acid of the 31-mer GR_pT524-pS617, except the pentaglycine section, was replaced in turn by alanine. Upon replacement of the phosphothreonine pT524 the binding to 14-3-3 decreased by 6700-fold, from K_d=18 nM to K_d=120 μM. Mutation of the phosphoserine pS617 had a less marked effect and led to a 72-

fold loss in potency resulting in a K_d of 1.3 µM. The two phosphoresidues are, as expected, the key residues in the binding by 14-3-3 to that doubly-phosphorylated peptide. P526 proved to be the most important non-phosphorylated residue with mutation of P526 resulting in an almost 70-fold decrease in potency (K_d=1.2 µM). Smaller effects were observed for R614 and K518, resulting in a 12-(K_d=220 nM) and 6-fold (K_d=110 nM) reduction in binding affinity, respectively (Table **1** and Supporting Table **S1**).

To further understand the role of pT524, a diphosphoserine analogue (GR_pS524-pS617) was synthesized. This peptide showed an 8-fold reduction in potency (K_d=140 nM) revealing the importance of the singular methyl group of T524. Even so, the affinity drop for pS524 to A524 was still more than an order of magnitude larger than the drop for the pS617 to A617 substitution, highlighting the unexpected relative importance of pT524 versus pS617. This is particularly surprising given the similar affinities for the two individual 13-mers but suggests that the artificial boundary conditions of the linked peptides influence one site more than the other. The potent binding of a diphosphorylated GR peptide with 14-3-3 is in line with the thermodynamic model for multivalency in 14-3-3 protein–protein interactions (30). The effect of the individual phosphosites on the strength of GR_pT524-pS617 binding could thus be simulated, assuming an average effective molarity value of 10 mM (Supporting Equation **S1**).

Crystallization of GR_pT524-pS617, GR_pT524 and GR_pS617 with 14-3-3ζ

The mechanistic details of the GR–14-3-3 interaction were further resolved by determining the crystal structures of 14-3-3ζ in complex with GR_pT524, GR_pS617, and GR_pT524-pS617. GR_pT524 was co-crystallized with 14-3-3ζ and the crystal structure was solved to a resolution of 2.09Å [Protein Data Bank (PDB) code 6YO8]. This high-resolution crystal structure allowed us to assign 12 out of 13 amino acids of the GR peptide. Two GR_pT524 peptides were found to bind the two respective central binding channels of one 14-3-3 dimer in an extended conformation. Details of the interaction showed that electrostatic effects dominated, with pT524 bound in the positively charged pocket of the 14-3-3 monomer made from K49, R56 and R127. Other polar contacts were observed between the peptide backbone and 14-3-3 residues, such as N173 and N224 (Table **2** and Supporting Fig. **S2a**).

The structure of GR_pS617 with 14-3-3ζ was solved to a resolution of 2.01Å (PDB code 6YMO). Similar to GR_pT524, two GR_pS617 peptides were observed to interact with one 14-3-3 dimer and pS617 made tight electrostatic contacts with the positively charged pocket of 14-3-3. Interestingly the electron density allowed us to assign only 6 out of 13 amino acids (Table **2** and Supporting Fig. **S2b**).

GR_pT524-pS617 was co-crystalized with 14-3-3ζ and the complex was solved to a resolution of 2.75Å (PDB code 6YOS). One diphosphorylated GR peptide was bound to one 14-3-3ζ dimer. The electron density allowed the assignment of 18 amino acid residues out of 31. The pentaglycine moiety was not visible in the electron density because of its flexibility. However, the distance between L528 and Y613, about 22Å, is sufficient to be bridged by 9 residues (Fig. **3a** and **3b**), supported by computational modelling of the pentaglycine linker (chapter 6 of the Supporting Information). The crystal structure of GR_pT524-pS617 interacting with 14-3-3ζ was consistent with the structures of GR_T524 and GR_S617 co-crystallized with 14-3-3ζ. The main interactions between the phosphorylated residues and 14-3-3 were in line with the GR_pT524-pS617 alanine scan results and previous published crystal structures of phosphopeptides interacting with 14-3-3 (25, 26). Many residues pointed their side-chains away from 14-3-3, consistent with

the observation from the alanine scan where mutation had a relatively small impact on the binding affinity with 14-3-3 (Fig. **3c** and Supporting Fig. **S2c-e**). A proline at position +2 relative to the phosphorylated serine/threonine residue, such as P526, is a common feature of 14-3-3 binding motifs 1 and 2 and this amino acid produces a sharp change in chain direction (9). P526 of GR_pT524-pS617 adopts a cis-conformation. On one side, it allows the carbonyl oxygen of L525 at the position +1 to form a hydrogen bond with the amino groups of K120 and N173. On the other side, P526 induces the peptide exit from the binding groove and avoids a clash of the remaining portion of the peptide with S45 and K49. The role of the proline in the structure was supported by the alanine scan. This turn creates a new pocket at the interface of the GR peptide and 14-3-3. Similarly, a second pocket is formed between GR residues 618-621 and the second 14-3-3 unit (Table **2** and Fig. **3**). Of note, an alternative orientation of GR_pT524-pS617 in the crystal structure with 14-3-3ζ could not be totally excluded and is described in the chapter 6 of the Supporting Information.

Assessment of the GR LBD phosphorylation profile by kinase screening

The two potential 14-3-3-binding phosphosites identified here, pT524 and pS617, are situated within the GR LBD. Hence, we aimed to test the binding affinity of doubly phosphorylated full-length GR LBD with 14-3-3. The kinase(s) responsible for phosphorylation of GR LBD have not yet been reported. We therefore aimed to identify the relevant kinase(s). The expression of WT human GR LBD from E. coli was unsuccessful, owing to solubility problems. Switching to the GR LBD mutant F602S (31) allowed us to express sufficient GR F602S N514-K777, in the presence of dexamethasone to be purified and used as a substrate for candidate kinases. The phosphorylation profile of GR LBD was determined in a radiometric protein kinase filter-binding assay (performed by ProQinase GmbH, Germany) in which the activity of 245 serine/threonine kinases was measured (Supporting Fig. **S3**). This phosphorylation profiling showed a differential ability of GR LBD to act as a substrate for the tested kinases (Supporting Fig. **S4**). We observed that 38 kinases displayed an activity ratio above 3 with 12 kinases above 5. MST2, MAP4K4, MST1 and TAOK2 were the kinases with the highest ratio, 19, 16, 14 and 13 respectively (Supporting Table **S2**). All of them belong to the STE20 kinase family, being upstream activators of the MAPK pathways. The 12 kinases with the highest activity ratios were selected for a follow-up assay and the phosphorylation profile of GR LBD by the 12 selected kinases was determined. MAP4K4, MINK1, MST1, MST2 and ROCK1 were observed to phosphorylate GR LBD (Supporting Fig. **S5**). The varying response may be due to the activity rate of the particular kinases having different kinetics under the chosen conditions and since the ATP concentration was fixed at 1 µM, regardless of the ATP-Km of each kinase.

Phosphorylation of GR LBD by MAP4K4, MINK1, MST1, MST2 and ROCK1 followed by enzyme digestion and analysis by mass spectrometry revealed different phosphorylation patterns (Table **3**). MAP4K4 showed mono- and diphosphorylation at T519 and T562. MST1 and MST2 both phosphorylated T562, T668, S682 and S746; each also phosphorylated additional sites, although these sites were markedly weaker in the LCMS analysis. MST2 showed a wider phosphorylation pattern than MST1 with up to seven phosphorylations observed. The two sites we had identified as most promising for 14-3-3 recognition (T524 and S617) were phosphorylated by MINK1 and ROCK1 respectively. In particular ROCK1 phosphorylated two different sites, T519 and S617, whilst MINK1 gave mainly mono and diphosphorylation of T524 and T562, with traces of phosphorylation at T635 (Table **3** and Supporting Fig. **S6**). Thus, the screening showed

that MINK1 and ROCK1 can phosphorylate GR T524 and S617, respectively, in vitro.

MINK1 phosphorylates GR LBD driving the interaction with 14-3-3

The ability of GR LBD, phosphorylated by either MINK1 or ROCK1, to interact with 14-3-3 was investigated. A far-Western blotting overlay assay was performed where we assessed the capacity of the different phosphorylated GR LBD, immobilized on a membrane, to bind the two recombinant yeast isoforms of 14-3-3 tagged with digoxygenin (BMH1-BMH2-digoxygenin). In this assay GR LBD phosphorylated by MINK1 showed direct interaction with 14-3-3 in a dose-dependent manner, whereas GR LBD phosphorylated by ROCK1 and the unphosphorylated GR LBD did not (Fig. **4b**), highlighting the specificity and sensitivity of the assays towards phosphorylated substrates.

MINK1 phosphorylates GR LBD at residues T524, T562 and to a lesser extent T635. T524 and T635 have been identified by the algorithm as plausible 14-3-3 binding sites with T561 but not T562. The 13-mer peptide centered on pT562 showed a weak interaction with 14-3-3ζ (K_d=200 µM). Interestingly, the 51-mer peptide GR_pT524-pT562, consisting of the two 13-mer peptides GR_pT524 and GR_pT562 with the native sequence as a linker, did not show a similar avidity effect as previously observed for GR_pT524-pS617. No significant trend has been reported between the effective molarity and the linker length (30, 32). Instead, the effective molarity depends on the flexibility of the linker between the two different binding sites. Thus, the binding affinity of GR_pT524-pT562 with 14-3-3ζ (K_d=23 and 15 µM, measured by FP and SPR respectively) and its low effective molarity (0.2 mM) might suggest a more structured linker. Crystal structure analysis (PDB code 1M2Z) placed GR T562 in the helix 3 which forms the spine of the protein. It would be unlikely that this helix changes its structure, questioning the ability of GR T562 to interact with 14-3-3 proteins.

Interaction between full length GR and 14-3-3

The interaction between full length GR and 14-3-3 was investigated in a cellular system to validate the relevance of the peptide studies. In an initial experiment, HEK293 and U2OS cells were transiently transfected with WT GR and, after overnight starvation, the cells were treated with a panel of stimuli that have previously been shown to promote phosphorylation of 14-3-3-binding sites of other target proteins (33). Results from co-immunoprecipitation (Co-IP) experiments and far-Western blotting overlay assay showed that GR interacted with 14-3-3 proteins upon stimulation with forskolin (a cell-permeable diterpenoid which activates adenylyl cyclase, increases intracellular cAMP concentration and thus activates protein kinase A (PKA)) and calyculin A (a cell-permeable potent and selective protein phosphatase inhibitor) (Supporting Fig. **S7**).

The role of the previously identified GR phosphosites in the binding with 14-3-3 was investigated in cells. U2OS cells were transiently transfected with WT GR or the GR double mutant, T524A S617A, before treatment with calyculin A. Under our experimental conditions, Co-IP and far-Western blotting overlay experiments revealed a significant decrease, about 35%, of the interaction between 14-3-3 and GR double mutant as compared to WT GR (Fig. **4c** and **4d**). These results confirm the interaction between GR and 14-3-3 and highlight the importance of the phosphorylation of the two GR residues T524 and S614.

Upon stimulation with forskolin or calyculin A, MINK1 also interacts with 14-3-3 (Supporting Fig. **S8**) (consistent with unpublished data by Gavuthami Murugesan and CM, University of Dundee). Thus, the GR–14-3-3 interaction and the MINK1–14-3-3 interaction are both promoted in parallel in cells stimulated with

forskolin and calyculin A (Supporting Fig. **S7**). We established that U2OS cells have a very low endogenous expression of MINK1, as no signal from this kinase could be detected by Western blotting (Supporting Fig. **S9**). Therefore, U2OS cells were either transfected with WT GR or co-transfected with WT GR and MINK1. In the absence of further stimulation, no GR–14-3-3 interaction was observed in either cells. Stimulation with calyculin A increased the level of phosphorylated GR by preventing GR dephosphorylation, so that the protein was capable of binding to 14-3-3 in a far-Western overlay. This interaction increased, by about 70%, in the presence of overexpressed MINK1 (Fig **4e** and **4f**). Together these results suggest that activated MINK1 kinase phosphorylates GR and triggers the GR–14-3-3 protein–protein interaction.

Discussion

In this study, we systematically investigated the GR–14-3-3 interaction at a GR peptide level, using biophysical assays, alanine scanning and X-ray crystallography. We particularly focused on 14-3-3σ and 14-3-3ζ, two very representative isoforms, since the seven 14-3-3 isoforms hold a high sequence similarity, notably in the amphipathic binding groove (34). Two GR phosphorylation sites, within the GR LBD, were identified as mediating the strongest binding to 14-3-3: T524 and S617. GR LBD has been previously reported to interact with 14-3-3, using yeast two hybrid assays, GST pull-down and Co-IP experiments, whilst GRβ isoform, which shares the same N-terminal and DNA binding domain but contains a different LBD, did not (14, 19, 20). 14-3-3 binding sites are mostly located within intrinsically disordered (ID) regions or bordering the functional domains (35). Interestingly, GR residue T524 was anticipated to be within an ID region (globplot.embl.de) and crystal structure analysis of GR LBD placed this residue within a random coil (36). S617 was found in a relatively disordered area, i.e. the loop between helix 5 and β-sheet 1, but within an ordered domain, which to the best of our knowledge, might be one of the first examples of a 14-3-3 binding site located in ordered regions. Mechanistically, after phosphorylation, 14-3-3 partners bind in the amphipathic groove of 14-3-3, leading to a disorder-to-order transition, entropically disadvantageous, but enthalpically favorable, driven by the formation of charge-charge interactions with the phosphate group and hydrogen bonding to neighboring residues (35).

One site, GR S134, previously reported to be a 14-3-3 recognition site and predicted by the algorithm used in this study, matches the mode 1 binding motif, RSX-pS/T-XP where X is any amino acid (cysteine excluded) and pS/T is a phosphorylated serine or threonine. Phosphorylation of GR S134, upon oxidative stimuli, was found to enhance GR interaction to 14-3-3 proteins (18). Here, we report that GR_pS134 interacts with the ζ and σ isoforms of 14-3-3 but with a weaker binding affinity than the two identified sites from GR LBD.

The dimeric GR_pT524-pS617 peptide revealed an impressive avidity gain over the monomeric components with a low nanomolar affinity toward 14-3-3. Examination of the crystal structure of GR LBD showed that T524 and S617 are both solvent exposed, and that the distance between these two residues in the crystal structure is 37Å, closely corresponding to the distance between the two phospho binding sites of 14-3-3. Other steroid hormone receptors, however, such as the androgen and the mineralocorticoid receptors, undergo a N/C interaction for complete transcriptional activity (37, 38). Full length GR has not been crystallized yet and an interdomain interaction through 14-3-3 binding, namely an interaction between NTD, such as S134, and LBD of GR, could be envisioned. Our biophysical assays showed that the affinity of GR_pS134-pT524, although 15-fold weaker than GR_pT524-pS617, is still in the sub-micromolar range (K_d=0.55 µM) which cannot exclude a potential interaction of GR pS134 with 14-3-3. In addition, cell-based approaches revealed that the affinity between GR double mutant, T524A S617A, and 14-3-3 decreased by 35% as compared to WT GR, but was not abolished. These results suggest that 14-3-3 interacts with GR through multiple sites. Further experiments would be necessary to fully quantify the individual effect of the GR phosphosites in 14-3-3 binding with full length GR as well as their biological role by monitoring GR translocation, GR transcriptional activity or GR protein level.

14-3-3 has been shown to interact with various nuclear hormone receptors and modulate their activity, adding another layer of regulation beyond ligand-driven activation. 14-3-3 Interaction with ERRγ, upon S179 phosphorylation, favors ERRγ cytoplasmic localization, alters its transcriptional activity and

its ability to promote hepatic gluconeogenesis (12). 14-3-3 Interaction with ERα, upon T594 phosphorylation, inhibits ERα dimerization and transactivation (11). Interaction of 14-3-3 with PXR leads to the overexpression of P-glycoprotein (also known as multidrug resistance protein 1) (13). Previous studies on GR–14-3-3 protein–protein interaction have reported on the 14-3-3 modulation of GR activity, with different consequences assigned, including GR translocation and GR transcriptional activity (14, 16–20). These studies focused on distinct 14-3-3 isoforms and different cellular contexts which could explain the seemingly conflicting results. The 14-3-3 isoforms indeed interact with different protein partners, have different affinities, distinct in vivo effects on targets and a specific tissue distribution (39–41). GR has been reported to dimerize through amino acids found in GR DBD and GR LBD such as residues P625 and I628 (42, 43). These two residues are closely located to the 14-3-3 binding site of GR, S617, and it is enticing to speculate that phosphorylation of S617 and interaction with 14-3-3 would negatively impact GR dimerization. To the best of our knowledge, however, no study on the role of 14-3-3 in GR dimerization has been reported. Co-crystallization of GR_pT524-pS617 with 14-3-3ζ led to the identification of two new binding pockets created at the interface of the GR peptide and 14-3-3 protein. It is enticing to speculate that these pockets (pocket size estimation of 390$Å^3$) could be exploited to find a molecule that would form positive interactions with each partner, acting as a “molecular glue” to stabilize the GR–14-3-3 protein–protein interaction. Such a tool compound could play a significant role in the quest to understand the physiological role of the GR–14-3-3 protein–protein interaction.

It is of great interest to fully unravel the underlying signaling network of GR, owing to the enormous importance of GR drugs and their widespread use, despite their many side-effects. Collectively our results contribute to answering the long-standing question on the 14-3-3 regulation of GR signaling pathways and highlight both MINK1 and the GR–14-3-3 axis as potential targets for future therapeutic intervention.

Experimental procedures

Material, instruments, reagents, antibodies and plasmids

Detailed information is provided in Supporting Information.

Peptide synthesis

General Protocol for SPPS. The peptides were synthesized via Fmoc/tBu solid-phase peptide. The first amino acid was attached to the 2-Chlorotrityl chloride resin following **method A** to reach a loading of 0.66 mmol/g. The peptide chains were then assembled according to **method B**. The peptides were then labelled by either addition of a fluorescein isothiocyanate (FITC) tag (**method C**) or N-terminal acetylation (**method D**) before being cleaved from the resin, deprotected according to **method E** and purified.

Method A: Attachment of the first amino acid on the 2-Chlorotrityl chloride resin. 2-Chlorotrityl chloride resin (0.3-0.8 meq/g, final loading 0.66 mmol/g) was swollen in DCM for 10 min and then the solvent was drained. The first amino acid (1 eq) was dissolved in DCM (1 mL) and DIPEA (3 eq) was added. The solution was added to the resin and stirred at room temperature under nitrogen bubbling. After 10 min DIPEA (7 eq) was added to the resin and the reaction mixture was stirred for 40 min. MeOH (0.8 µL/mg of resin) was added to the resin and was stirred for 10 min. The mixture was drained, and the resin was washed with DMF (3 ×) and DCM (3 ×).

Method B1: Automated Fmoc SPPS, Biotage® Initiator+ AlstraTM automated microwave peptide synthesizer. The resin was swollen with DMF (2 ×) and the Fmoc Nα-protecting group was removed with 20% piperidine in DMF (2 ×; 3 min then 10 min) at room temperature. The amino acids dissolved in DMF (0.3 M) were repeatedly coupled with HATU (3 eq) in NMP (0.5 M) and DIPEA (6 eq) in NMP (2 M) at room temperature for 45 or 60 min. The resin was finally washed with DCM (6 ×).

Method B2: Automated Fmoc SPPS, Biotage® Syro II automated parallel peptide synthesizer. The resin was swollen with DMF (6 ×) and the Fmoc Nα-protecting group was removed with 40% piperidine in DMF (3 min) followed by 20% piperidine in DMF (10 min) at room temperature. The amino acids (4 eq) dissolved in DMF (0.5 M) were repeatedly coupled with HATU (4 eq) in DMF (0.48 M) and DIPEA (8 eq) in NMP (2 M) at room temperature for 40 min. The resin was finally washed with DCM (3 ×), MeOH (3 ×) and Et2O (3 ×).

Method C: Addition of a fluorescein isothiocyanate (FITC) tag at the N terminal position. After the final Fmoc deprotection, the resin was swollen with DCM (2 ×). In the dark, FITC (3 eq) was dissolved in DMF and HATU (3 eq) and DIPEA (4.5 eq) were added. The reaction mixture was added to the resin and stirred at room temperature under nitrogen bubbling for 45 min. The mixture was drained, and the resin was washed with DMF (3 ×) and DCM (3 ×).

Method D: Acetylation of the N terminal position. After the final Fmoc deprotection, the resin was swollen with DCM (2 ×). A solution of acetic anhydride (10 eq) and DIPEA (10 eq) in DMF was added to the resin and stirred at room temperature under nitrogen bubbling for 15 min before the mixture was drained. This procedure was repeated twice, and the resin was washed with DMF (3 ×) and DCM (3 ×).

Method E: Cleavage from resin/side-chain deprotection. A solution of TFA/water/EDT/TIS 94:2.5:2.5:1 (5 mL) was added to the dry resin. The reaction mixture was shaken at room temperature for 3 h. TFA solution was then collected in cold diethyl ether. The resin was rinsed with TFA (1 mL, 3 ×) and the TFA solution collected. The precipitated

peptide was centrifuged, and the crude peptide was lyophilized from acetonitrile-water.

14-3-3 full length expression and purification

The σ and ζ isoforms of human 14-3-3 were cloned in pProEx Htb vector as 6His-Linker (MSYYHHHHHHDYDIPTTENLYFQGAMGS)-h14-3-3 and expressed in E. coli BL21 (DE3)STAR competent cells. Cultures were grown in Terrific Broth media supplemented by 3 mM $MgCl_2$, 0.02% glucose, 0.8% glycerol and 50 µg/mL carbenicillin at 37 °C to an OD_{600} of 0.4-0.6 and then induced overnight with 0.4 mM of IPTG at 18 °C to reach an OD_{600} higher than 20. Cells were harvested by centrifugation (5 000g, 20 min) and lysed using a cell disruptor (Constant Systems LTD) at 25 KPSI in lysis buffer containing 50 mM Tris, 300 mM NaCl, 12.5 mM imidazole, 1 mM TCEP, 5 mM $MgCl_2$ and 1 tablet protease inhibitor Roche per 100 mL of lysis buffer. After centrifugation (35 000g, 45 min), the lysate was incubated with Ni-NTA derivatized Sepharose resin (Qiagen) overnight at 4 °C. The nickel-resin was washed with buffer containing 0.1% triton X-100 then with lysis buffer and the proteins were eluted with buffer containing 250 mM imidazole. 14-3-3 proteins were further purified by size exclusion chromatography on a Hiload 26/60 Superdex 75 per grade (Pharmacia Biotech) using HBS P+ buffer (10 mM HEPES pH 7.4, 150 mM NaCl, 0.005% v/v Tween-P20). The correct fractions were combined, concentrated, aliquoted, frozen in liquid nitrogen and stored at -80 °C.

14-3-3 ΔC expression and purification

Human 14-3-3ζΔC (C-terminally truncated, including residues 1-231, for crystallography purposes) was cloned in pProEx Htb vector and expressed in E. coli BL21 (DE3) competent cells. Cultures were grown in TB media at 37 °C to an OD_{600} of 0.8-1 and then induced overnight with 0.4 mM of IPTG at 18 °C to reach an OD_{600} higher than 20. Cells were harvested by centrifugation (10 000 g, 15 min) and lysed using a cell disruptor (Avestin EmulsiFlex C3 Homogenizer) at 20 KPSI in lysis buffer containing 50 mM Tris, 300 mM NaCl, 12.5 mM imidazole and 2 mM β-mercaptoethanol. After centrifugation (40 000 g, 30 min), the lysate was applied to a HisTrap HP column (GE), washed with lysis buffer and the 14-3-3 proteins were eluted with 50 mM Tris, 300 mM NaCl, 250 mM imidazole and 2 mM β-mercaptoethanol. The right fractions were combined, and the full-length proteins were dialyzed and rebuffered in 25 mM HEPES pH 7.5, 100 mM NaCl, 10 mM $MgCl_2$, 0.5 mM Tris(2-carboxyethyl)phosphine. The His Tag was removed via TEV cleavage. The cleavage solution was applied to the HisTrap HP column to remove the TEV protease. The protein was further purified via size exclusion chromatography on a Superdex75 (GE) using the following buffer: 20 mM Tris pH 7.4, 150 mM NaCl and 2 mM β-mercaptoethanol. The correct fractions were combined, concentrated, aliquoted, frozen in liquid nitrogen and stored at -80°C.

GR LBD expression and purification

GR N514-K777 and GR F602S N514-K777 were cloned in pET24a base vector as N-terminal 6His tag with adjacent TEV cleavage site (ENLYFQG) and expressed in E. coli BL21 (DE3)STAR competent cells. Cultures were grown in TB media 5052 auto induction: TB media supplemented by 3 mM $MgCl_2$, 0.05% glucose, 0.5% glycerol, 0.2% lactose, 100 µg/mL kanamycin and 100 µM dexamethasone at 37 °C to an OD_{600} of 1 and then induced for 48 h at 16 °C. The culture was centrifuged (5 000 g, 20 min) and the pellet was lysed using a cell disruptor (Constant Systems LTD) at 25 KPSI in lysis buffer containing 50 mM Tris pH 8, 1% CHAPS, 10% glycerol, 1 mM TCEP, 50 µM dexamethasone and 1 tablet protease inhibitor Roche per 100 mL of lysis buffer. The lysate was incubated with Ni-NTA derivatized Sepharose resin (Qiagen) overnight at 4 °C washed with buffer containing 60 mM NaCl, 30 mM imidazole and eluted with buffer containing

30 mM NaCl, 300 mM imidazole. GR LBD proteins were further purified by size exclusion chromatography on a Hiload 16/60 Superdex 75 per grade (Pharmacia Biotech) using the following buffer: 50 mM Tris pH 9, 1 mM TCEP and 25 µM dexamethasone. The correct fractions were combined, concentrated, aliquoted, frozen in liquid nitrogen and stored at -80 °C.

Fluorescence polarization (FP) assay with GR phosphorylated peptides and 14-3-3

The FITC labelled peptides were solubilized to a final concentration of 60 nM (for the mono phosphorylated peptides) or 10 nM (for the doubly phosphorylated peptides) and were titrated with 14-3-3ζ or 14-3-3σ in concentration dilution series from 300 µM or 150 µM, depending on the binding affinity of the peptide, in a 384-well flat bottom black polypropylene microplate (Greiner Bio-One). Following 30-minute incubation at room temperature, the plates were read on a plate reader PHERAstar (BMG LABTECH GmbH) for FP signal using white light and standard excitation (485 nm) and emission (520 nm). Measurements were performed as triplicates. Binding data were fit to a standard Hill equation using the software Genedata Screener®. The figures were made using the software GraphPad Prism 8. Fluorescence polarization data were expressed as millipolarization (mP) units and the dynamic range (ΔmP) was the difference of the signals from bound peptide and free peptide. Errors are standard error of the fit.

Surface plasmon resonance (SPR) assays with GR phosphorylated peptides and 14-3-3

SPR binding assays were performed using a Biacore 3000 (GE Healthcare). 6His tagged 14-3-3 proteins (3 µM) were immobilized on a SPR sensorchip NTA derivatized carboxymethyl dextran hydrogel (Xantec Bioanalytics) at 4000 RU for 14-3-3σ and 2000 RU for 14-3-3ζ according to the manufacturer's instructions. A 96-well V-shaped polypropylene microtiter plate was prepared with different GR peptides concentrations in HBS P+ buffer and normalized to 1 or 3% v/v DMSO, depending on the maximum peptide concentration, using the HP D300 Digital Dispenser (Hewlett-Packard Company). In the dose response assay, ten dilutions of GR peptide from 300 µM or 45 µM, depending on the peptide binding affinity, were performed. The peptide samples were injected using the HBSP+ buffer with 1 or 3% v/v DMSO at a continuous flow rate of 20 µL/min for 1 min on the immobilized 14-3-3 and before the next injection 2.5 min after. An extra waiting time of 12.5 min was set to allow complete dissociation of the doubly phosphorylated peptides. Measurements were performed as triplicates. When necessary data were corrected using a solvent correction curve. Binding data were fit to a standard Hill using the software Genedata Screener® and the figures were made using the software GraphPad Prism 8. Errors are standard error of the fit.

X-ray crystallography studies

Sitting drop co-crystallization of 14-3-3ζ and GR peptides. Crystals were grown using the sitting drop vapor diffusion crystallization method by mixing 14-3-3ζΔC with a mono-phosphorylated GR peptide in a 1:2 ratio or with a doubly phosphorylated peptide in a 1:1 ratio with a resulting protein concentration of 10 mg/mL in a crystallization buffer containing 20 mM HEPES pH 7.5, 2 mM $MgCl_2$ and 2 mM DTT. Sitting drops were formed by mixing equal volumes of protein/peptide solution and precipitant (2 × 100 nL) on a 96-well Art Robbins Flat Ledge plate (Hampton Research) using a nanoliter liquid handler mosquito® (SPT Labtech) and equilibrated over a 80 µL reservoir at 4 or 20 °C. Crystals were harvested after a few days, soaked in cryo-protectant containing the precipitant supplemented with 20% v/v glycerol and flash-cooled in liquid nitrogen before data collection. The precipitant solutions are listed below.

GR_pT524 co-crystallized with 14-3-3ζ: The crystals were grown at 4 °C using a precipitant solution (1.29 M $MgCl_2$, 22.5% PEG 3350, 0.1 M Tris pH 8.3) supplemented with 10% of an additive containing 40% v/v of 2,5-Hexanediol. The crystals were haverested after 8 days. **GR_pS617 co-crystallized with 14-3-3ζ:** The crystals were grown at 4 °C using a precipitant solution (2.04 M ammonium sulfate, 0.2 M sodium citrate) supplemented with 10% of an additive containing 0.33% w/v 3-aminobenzoic acid, 0.33% w/v 3-aminosalicylic acid, 0.33% w/v salicylic acid and 0.02 M HEPES sodium pH 6.8. The crystals were haverested after 5 days. **GR_pT524-pS617 co-crystallized with 14-3-3ζ:** The crystals were grown at 20 °C using a precipitant solution (0.35 M $MgCl_2$, 24.4% PEG 3350, 0.1 M Bis Tris pH 5.5) supplemented with 10% of an additive containing 0.06 M CHAPS, 0.06 M HEPES, 0.06 M Tris, 0.25% w/v Hexamminecobalt(III) chloride and 0.02 M HEPES sodium pH 6.8. The crystals were haverested after 8 days.

Data collection and processing. Diffraction data were collected at the European Synchrotron Radiation Facility (ESRF) in Grenoble, France (0.976Å, 100 K, ESRF Beamline ID30B) and at Diamond Light Source (DLS) at the Harwell Science and Innovation Campus in Oxfordshire, UK (0.916Å, 100 K, DIAMOND Beamline I04-1). Molecular replacement was performed using Phaser from the ccp4i package and refinement and manual rebuilding was done using Buster and Coot software packages. The structures (PDB codes: 6YO8, 6YMO and 6YOS) were refined to a resolution of 2.09Å, 2.01Å and 2.75Å with Rwork/Rfree factors of 0.224/0.235, 0.212/0.228 and 0.268/0.291, respectively. X-ray diffraction data collection and structure refinement statistics are summarized in Table **2**. The figures were made using the software PyMol (DeLano Scientific LLC).

Radiometric protein kinase filter-binding assay

The kinase screen was performed by ProQinase GmbH, Freiburg im Breisgau, Germany. A radiometric protein kinase filter-binding assay was used for measuring the kinase activity of the 245 serine/threonine kinases. The reaction cocktails were pipetted into 96-well V-shaped polypropylene microtiter plates in the following order: kinase solution (10 µL) and buffer/ATP/test sample mixture (40 µL). The reaction cocktails contained 60 mM HEPES-NaOH pH 7.5, 3 mM $MgCl_2$, 3 mM $MnCl_2$, 3 µM Na-orthovanadate, 1.2 mM DTT, 1 µM ATP/[γ-33P]-ATP (8.68 × 1005 cpm per well), protein kinase (1-400 ng/50 µL) and sample protein (5 µg/50 µL) with minor modifications as stated in the Supporting Information. Each assay plate comprised one well for a buffer/substrate control containing no enzyme. The assay plates were incubated at 30 °C for 60 min and the reaction cocktails were stopped with 20 µL of 10% v/v H_3PO_4. The reaction cocktails were transferred into 96-well glass-fiber filter plates (MultiScreen MSFC, Millipore), pre-wetted with 150 mM H_3PO_4, followed by 10 min incubation at room temperature. After washing with 250 µL of 150 mM H_3PO_4 (3 ×) and with 20 µL of 100% ethanol and drying for 30 min at 40 °C, 50 µL of scintillator (Rotiszint Eco plus, Roth) were added to each well and incorporation of ^{33}Pi ("counting of cpm") was determined with a microplate scintillation counter (Microbeta, Perkin Elmer).

Peptide mapping

The protein samples were phosphorylated as described above with non-radioactive ATP. 10, 5, 3, 1 µg of protein sample, supplemented with 25% NuPAGE™ LDS Sample Buffer (4 ×) and 10% NuPAGE™ Sample Reducing Agent (10 ×), was run on a NuPAGE™ 4-12% Bis-Tris Protein Gels, 1.0 mm with MOPS buffer and the bands were reveal using Coomassie Brilliant Blue. Bands of interest were cut from the gel to be washed with water, 1:1 acetonitrile/water, 100 mM ammonium bicarbonate, 1:1 acetonitrile/100 mM ammonium bicarbonate

successively for 10 min. The bands were reduced and alkylated with a solution of 10 mM DTT in 100 mM ammonium bicarbonate for 45 min at 65 °C followed by a solution of 50 mM iodoacetamide in ammonium bicarbonate for 20 min in the dark. The samples were washed with 50 mM ammonium bicarbonate, 1:1 100 mM ammonium bicarbonate/acetonitrile and 100% acetonitrile successively for 10 min and dried. The bands were digested with 10 ng/µL trypsin and 12.5 ng/µL chymotrypsin in 50 mM ammonium bicarbonate at room temperature overnight. The material was extracted twice with 0.1% TFA/60% acetonitrile then dried before being analyzed by mass spectrometry. The data files generated were searched against the in-house or Swissprot database using the software Mascot Daemon. The searches were then manually verified.

Intact mass

The protein samples were phosphorylated as described above with non-radioactive ATP. The samples were diluted to 0.01 mg/mL in 0.1% formic acid and 5% acetonitrile and were analyzed by mass spectrometry. The TIC peak data was used to generate the m/z spectrum and the data were deconvoluted to give final mass.

Database search parameters and acceptance criteria for identifications

Search engine and release version: Mascot Daemon Version 2.7.0

Sequence database searched: SwissProt, Human

Release version/date of sequence database searched: August 2018

Number of entries in the database actually searched: Whole of human swissprot database

Specificity of all proteases used to generate peptides: Trypsin and chymotrypsin. Trypsin specificity is C-terminal side of lysine and arginine unless there is a proline on the carboxyl side. Chymotrypsin's main cleavage sites are after tryptophan, tyrosine and phenylalanine.

Number of missed and/or non-specific cleavages permitted: 2

Fixed modifications (including residue specificity) considered: Carbamidomethylation on cysteine (+57.021)

Variable modifications (including residue specificity) considered: Oxidised methionine (+15.995Da), Phosphorylation of threonine, serine, tyrosine (+15.966Da)

Mass tolerance for precursor ions: +/- 0.6 Da

Mass tolerance for fragment ions: +/- 0.6 Da

Threshold score/Expectation value for accepting individual spectra: 20

Cell culture, transfection and stimulation

The HEK293 and U2OS cell lines (ATCC) were cultured in DMEM medium, supplemented with 10% foetal bovine serum and 1% penicillin-streptomycin (10,000 U/mL) at 37 °C in a 5% CO_2 environment. For Co-IP assay, 3 × 106 cells were seeded in a 15 cm cell culture dish. At 60–70% confluence, the HEK293 cells were transiently transfected with a mixture of 6 µg GFP- MINK1 or GFP-GR DNA and 24 µL lipofectamine 2000 in 2 mL Opti-MEM for 24 h. At 60–70% confluence, the U2OS cells were transiently transfected with a mixture of 8 µg GFP-MINK1 or GFP-GR and/or FLAG-MINK1 DNA and 32 µL X-tremeGENE™ 9 DNA in 2 mL Opti-MEM for 24 h. Stimulation with forskolin, H89, IGF-1 and PI303 was preceded by a cell starvation step where the cells were incubated with DMEM medium without supplement overnight. The cells were treated with the right compound at the concentration and during the time stated in the table found in the Supporting Information.

Co-immunoprecipitation assay

Cells were collected and lysed in radioimmunoprecipitation assay (RIPA) buffer containing 50 mM Tris-HCl pH8, 150 mM NaCl, 1 mM EDTA, 0.1% SDS, 1% Na deoxycholate, 1% NP-40 supplemented with protease inhibitor cocktail. After lysis, the concentration of protein was quantified by Bradford test. Dilution/washing buffer containing 50 mM Tris-HCl pH8, 150 mM NaCl and 1 mM EDTA was added to reach equal concentration and 50 µL were saved as input fraction for future analysis. Equal volumes of protein solution were incubated with 10 µL GFP-Trap Agarose beads® (ChromoTek) at 4 °C for 2 h. 50 µL were saved as flowthrough fraction for future analysis and the beads were washed with dilution/washing buffer (2 ×). 30 µL NuPAGE™ LDS Sample Buffer (4 ×) were added to the beads and proteins from the input, flowthrough and IP fractions were denatured at 95 °C for 5 min.

Eluted proteins were resolved on a NuPAGE™ 4-12% Bis-Tris Protein Gels, 1.0 mm. The gels were transferred to polyvinylidene difluoride (PVDF) membranes (previously activated in methanol) which were then blocked with Intercept® (TBS) blocking buffer (LI-COR). After washing with TBST, the membranes were probed at 4 °C overnight with the primary antibodies listed in Supporting Information. After washing with TBST, the membranes were incubated with the specific rabbit IRDye 800CW secondary antibody (LI-COR) for 1 h at room temperature. After washing with TBST, the blots were detected using an Odyssey CLx Imaging system (LI-COR). Data analysis was performed using Image Studio (LI-COR).

Far-Western blot assay

Samples containing proteins from Co-IP assay or GR LBD in vitro phosphorylated were loaded on a NuPAGE™ 4-12% Bis-Tris Protein Gels, 1.0 mm and separated. The gels were transferred to polyvinylidene difluoride membranes which were blocked with Intercept® (TBS) blocking buffer (LI-COR). After washing with TBST, the membranes were probed at 4 °C overnight with BMH1-BMH2-digoxygenin probe diluted in 5% bovine serum albumin (BSA) TBST. After washing with TBST, the membranes were incubated with anti-digoxigenin antibody (R&D Systems) at 4 °C overnight. After washing with TBST, the membranes were incubated with the specific mouse IRDye 800CW or IRDye 680LT secondary antibody (LI-COR) for 1 h at room temperature. After washing with TBST, the blots were detected using an Odyssey CLx Imaging system (LI-COR). Data analysis was performed using Image Studio (LI-COR). Measurements were performed as triplicates. The figures were made using the software GraphPad Prism 8.

Experimental Design and Statistical Rationale

Individual data points are shown when possible, and always for $n \leq 20$. Clearly defined error bars are present, representing the standard deviation of three independent experiments.

For the investigation of the interaction between full length GR and 14-3-3, Western blot quantification was obtained using Image Studio (LI-COR) from three independent cell-based assays. The significance (two-tailed p value) was assessed by t-test. Asterisks were attributed for the following significance values: *$p < 0.05$, ****$p < 0.0001$.

Data availability

The authors declare that all data supporting the findings of this study are available within the paper and its Supporting information files.

The mass spectrometry proteomics data have been deposited to the ProteomeXchange Consortium via the PRIDE (44) partner repository with the dataset identifier PXD022364 and 10.6019/PXD022364

Acknowledgments

The authors thank Dr. Anais Noisier for her help with peptide synthesis, Dr. Anna-Carin Carlsson, Dr. Linda Thunberg and Annika Langborg Weinmann MSc from the Separation Science Laboratory team for their support with peptides purification, ProQinase GmbH for the kinase screen, Dr. Anna Hoyle for her help with peptide mapping as well as Dr. Ian Ganley, Dr. Stefan Vollmer and Dr. Sofia Winslow for their assistance in cell-based assays. The authors acknowledge ESRF and DLS for providing access to their beamlines and Dr. Werngard Czechtizky for generous support of the project.

Author contributions

The authors contributed in the following manner: MWDP conceived and directed the project, CCM performed peptide synthesis and purification, CCM and AG the biophysical experiments and analyses, CCM and LW co-crystallized GR peptides with 14-3-3. CCM, LDM, KE and CO determined and analyzed the X-ray crystal structure and made relevant figures and tables. CCM and AS performed protein production and purification, CCM and MWDP analyzed the kinase screening. CCM, ML and CM performed the cell-based assays and analyses. CCM, LB, CO and MWDP drafted relevant parts of the manuscript. All authors made comments on the manuscript and approved the final version.

Funding and additional information

This work was supported by the Initial Training Network TASPPI, funded by the H2020 Marie Curie Actions of the European Commission under Grant Agreement 675179.

Conflict of interest

LDM, KE, AG, AS, LW and MWDP are employed by and/or own shares in AstraZeneca.

References

1. Kino, T. (2018) GR-regulating Serine/Threonine Kinases: New Physiologic and Pathologic Implications. *Trends Endocrinol. Metab.* **29**, 260–270

2. Cain, D. W., and Cidlowski, J. A. (2017) Immune regulation by glucocorticoids. *Nat. Rev. Immunol.* **17**, 233–247

3. Souffriau, J., Eggermont, M., Van Ryckeghem, S., Van Looveren, K., Van Wyngene, L., Van Hamme, E., Vuylsteke, M., Beyaert, R., De Bosscher, K., and Libert, C. (2018) A screening assay for Selective Dimerizing Glucocorticoid Receptor Agonists and Modulators (SEDIGRAM) that are effective against acute inflammation. *Sci. Rep.* **8**, 12894

4. Kuna, P., Aurivillius, M., Jorup, C., Prothon, S., Taib, Z., and Edsbäcker, S. (2017) Efficacy and Tolerability of an Inhaled Selective Glucocorticoid Receptor Modulator – AZD5423 – in Chronic Obstructive Pulmonary Disease Patients: Phase II Study Results. *Basic Clin. Pharmacol. Toxicol.* **121**, 279–289

5. Scheschowitsch, K., Leite, J. A., and Assreuy, J. (2017) New insights in glucocorticoid receptor signaling-more than just a ligand-binding receptor. *Front. Endocrinol. (Lausanne).* **8**, 16

6. Weikum, E. R., Knuesel, M. T., Ortlund, E. A., and Yamamoto, K. R. (2017) Glucocorticoid receptor control of transcription: Precision and plasticity via allostery. *Nat. Rev. Mol. Cell Biol.* **18**, 159–174

7. Deroo, B. J., Rentsch, C., Sampath, S., Young, J., DeFranco, D. B., and Archer, T. K. (2002) Proteasomal Inhibition Enhances Glucocorticoid Receptor Transactivation and Alters Its Subnuclear Trafficking. *Mol. Cell. Biol.* **22**, 4113–4123

8. Pennington, K., Chan, T., Torres, M., and Andersen, J. (2018) The dynamic and stress-adaptive signaling hub of 14-3-3: emerging mechanisms of regulation and context-dependent protein–protein interactions. *Oncogene*. **37**, 5587–5604

9. Johnson, C., Crowther, S., Stafford, M. J., Campbell, D. G., Toth, R., and MacKintosh, C. (2010) Bioinformatic and experimental survey of 14-3-3-binding sites. *Biochem. J.* **427**, 69–78

10. Rubio, M. P., Geraghty, K. M., Wong, B. H. C., Wood, N. T., Campbell, D. G., Morrice, N., and Mackintosh, C. (2004) 14-3-3-affinity purification of over 200 human phosphoproteins reveals new links to regulation of cellular metabolism, proliferation and trafficking. *Biochem. J.* **379**, 395–408

11. De Vries-van Leeuwen, I. J., da Costa Pereira, D., Flach, K. D., Piersma, S. R., Haase, C., Bier, D., Yalcin, Z., Michalides, R., Feenstra, K. A., Jiménez, C. R., de Greef, T. F. a, Brunsveld, L., Ottmann, C., Zwart, W., and de Boer, A. H. (2013) Interaction of 14-3-3 proteins with the Estrogen Receptor Alpha F domain provides a drug target interface. *Proc. Natl. Acad. Sci. U. S. A.* **110**, 8894–8899

12. Kim, D. K., Kim, Y. H., Hynx, D., Wang, Y., Yang, K. J., Ryu, D., Kim, K. S., Yoo, E. K., Kim, J. S., Koo, S. H., Lee, I. K., Chae, H. Z., Park, J., Lee, C. H., Biddinger, S. B., Hemmings, B. A., and Choi, H. S. (2014) PKB/Akt phosphorylation of ERRγ contributes to insulin-mediated inhibition of hepatic gluconeogenesis. *Diabetologia*. **57**, 2576–2585

13. Kim, S. W., Md. Hasanuzzaman, Cho, M., Kim, N. H., Choi, H. Y., Han, J. W., Park, H. J., Oh, J. W., and Shin, J. G. (2017) Role of 14-3-3 sigma in over-expression of P-gp by rifampin and

paclitaxel stimulation through interaction with PXR. *Cell. Signal.* **31**, 124–134

14. Wakui, H., Wright, A. P. H., Gustafsson, J., and Zilliacus, J. (1997) Interaction of the Ligand-activated Glucocorticoid Receptor with the 14-3-3η Protein. *J. Biol. Chem.* **272**, 8153–8156

15. Widén, C., Zilliacus, J., Gustafsson, J. Å., and Wikström, A. C. (2000) Glucocorticoid Receptor Interaction with 14-3-3 and Raf-1, a Proposed Mechanism for Cross-Talk of Two Signal Transduction Pathways. *J. Biol. Chem.* **275**, 39296–39301

16. Kim, Y. S., Jang, S.-W., Sung, H. J., Lee, H. J., Kim, I. S., Na, D. S., and Ko, J. (2005) Role of 14-3-3η as a Positive Regulator of the Glucocorticoid Receptor Transcriptional Activation. *Endocrinology*. **146**, 3133–3140

17. Hwang, Y., An, H. T., Kang, M., and Ko, J. (2018) Roles of 14-3-3β and γ in regulation of the glucocorticoid receptor transcriptional activation and hepatic gluconeogenesis. *Biochem. Biophys. Res. Commun.* **501**, 800–806

18. Galliher-Beckley, A. J., Williams, J. G., and Cidlowski, J. A. (2011) Ligand-Independent Phosphorylation of the Glucocorticoid Receptor Integrates Cellular Stress Pathways with Nuclear Receptor Signaling. *Mol. Cell. Biol.* **31**, 4663–4675

19. Kino, T., Souvatzoglou, E., De Martino, M. U., Tsopanomihalu, M., Wan, Y., and Chrousos, G. P. (2003) Protein 14-3-3σ Interacts With and Favors Cytoplasmic Subcellular Localization of the Glucocorticoid Receptor, Acting as a Negative Regulator of the Glucocorticoid Signaling Pathway. *J. Biol. Chem.* **278**, 25651–25656

20. Habib, T., Sadoun, A., Nader, N., Suzuki, S., Liu, W., Jithesh, P. V., and Kino, T. (2017) AKT1 has dual actions on the glucocorticoid receptor by cooperating with 14-3-3. *Mol. Cell. Endocrinol.* **439**, 431–443

21. Henriksson, M. L., Francis, M. S., Peden, A., Aili, M., Stefansson, K., Palmer, R., Aitken, A., and Hallberg, B. (2002) A nonphosphorylated 14-3-3 binding motif on exoenzyme S that is functional in vivo. *Eur. J. Biochem.* **269**, 4921–4929

22. Petosa, C., Masters, S. C., Laurie, A., Pohl, J., Wang, B., Liddington, R. C., Bankston, L. a, and Fu, H. (1998) 14-3-3ζ Binds a Phosphorylated Raf Peptide and an Unphosphorylated Peptide via Its Conserved Amphipathic Groove. *J. Biol. Chem.* **273**, 16305–16310

23. Madeira, F., Tinti, M., Murugesan, G., Berrett, E., Stafford, M., Toth, R., Cole, C., MacKintosh, C., and Barton, G. J. (2015) 14-3-3-Pred: improved methods to predict 14-3-3-binding phosphopeptides. *Bioinformatics*. **31**, 2276–2283

24. Vandevyver, S., Dejager, L., and Libert, C. (2014) Comprehensive overview of the structure and regulation of the glucocorticoid receptor. *Endocr. Rev.* **35**, 671–693

25. Stevers, L. M., Lam, C. V, Leysen, S. F. R., Meijer, F. A., van Scheppingen, D. S., de Vries, R. M. J. M., Carlile, G. W., Milroy, L. G., Thomas, D. Y., Brunsveld, L., and Ottmann, C. (2016) Characterization and small-molecule stabilization of the multisite tandem binding between 14-3-3 and the R domain of CFTR. *Proc. Natl. Acad. Sci. U. S. A.* **113**, E1152–E1161

26. Bier, D., Bartel, M., Sies, K., Halbach, S., Higuchi, Y., Haranosono, Y., Brummer, T., Kato, N., and Ottmann, C. (2016) Small-Molecule Stabilization of the 14-3-3/Gab2 Protein-Protein Interaction (PPI) Interface. *ChemMedChem.* **11**, 911–918

27. Molzan, M., and Ottmann, C. (2012) Synergistic binding of the phosphorylated S233- and S259-

binding sites of C-RAF to One 14-3-3ζ dimer. *J. Mol. Biol.* **423**, 486–495

28. Kostelecky, B., Saurin, A. T., Purkiss, A., Parker, P. J., and McDonald, N. Q. (2009) Recognition of an intra-chain tandem 14-3-3 binding site within PKCε. *EMBO Rep.* **10**, 983–989

29. Obsil, T., Ghirlando, R., Klein, D. C., Ganguly, S., and Dyda, F. (2001) Crystal Structure of the 14-3-3ζ:Serotonin N-Acetyltransferase Complex: A Role for Scaffolding in Enzyme Regulation. *Cell*. **105**, 257–267

30. Stevers, L. M., de Vink, P. J., Ottmann, C., Huskens, J., and Brunsveld, L. (2018) A Thermodynamic Model for Multivalency in 14-3-3 Protein–Protein Interactions. *J. Am. Chem. Soc.* **140**, 14498–14510

31. Bledsoe, R. K., Montana, V. G., Stanley, T. B., Delves, C. J., Apolito, C. J., Mckee, D. D., Consler, T. G., Parks, D. J., Stewart, E. L., Willson, T. M., Lambert, M. H., Moore, J. T., Pearce, K. H., Xu, H. E., and Carolina, N. (2002) Crystal Structure of the Glucocorticoid Receptor Ligand Binding Domain Reveals a Novel Mode of Receptor Dimerization and Coactivator Recognition. *Cell*. **110**, 93–105

32. Krishnamurthy, V. M., Semetey, V., Bracher, P. J., Shen, N., and Whitesides, G. M. (2007) Dependence of effective molarity on linker length for an intramolecular protein-ligand system. *J. Am. Chem. Soc.* **129**, 1312–1320

33. Chen, S., Murphy, J., Toth, R., Campbell, D. G., Morrice, N. A., and Mackintosh, C. (2008) Complementary regulation of TBC1D1 and AS160 by growth factors, insulin and AMPK activators. *Biochem. J.* **409**, 449–459

34. Bartel, M., Schäfer, A., Stevers, L. M., and Ottmann, C. (2014) Small molecules, peptides and natural products: Getting a grip on 14-3-3 protein-protein modulation. *Future Med. Chem.* **6**, 903–921

35. Sluchanko, N. N., and Bustos, D. M. (2019) Intrinsic disorder associated with 14-3-3 proteins and their partners. in *Progress in Molecular Biology and Translational Science*, 1st Ed., pp. 19–61, Elsevier Inc., Cambridge, **166**, 19–61

36. Edman, K., Hosseini, A., Bjursell, M. K., Aagaard, A., Wissler, L., Gunnarsson, A., Kaminski, T., Köhler, C., Bäckström, S., Jensen, T. J., Cavallin, A., Karlsson, U., Nilsson, E., Lecina, D., Takahashi, R., Grebner, C., Geschwindner, S., Lepistö, M., Hogner, A. C., and Guallar, V. (2015) Ligand Binding Mechanism in Steroid Receptors: From Conserved Plasticity to Differential Evolutionary Constraints. *Structure*. **23**, 2280–2290

37. Li, J., Fu, J., Toumazou, C., Yoon, H. G., and Wong, J. (2006) A Role of the Amino-Terminal (N) and Carboxyl-Terminal (C) Interaction in Binding of Androgen Receptor to Chromatin. *Mol. Endocrinol.* **20**, 776–785

38. Pippal, J. B., Yao, Y., Rogerson, F. M., and Fuller, P. J. (2009) Structural and Functional Characterization of the Interdomain interaction in the Mineralocorticoid Receptor. *Mol. Endocrinol.* **23**, 1360–1370

39. Aghazadeh, Y., and Papadopoulos, V. (2016) The role of the 14-3-3 protein family in health, disease, and drug development. *Drug Discov. Today*. **21**, 278–287

40. Benzinger, A., Popowicz, G. M., Joy, J. K., Majumdar, S., Holak, T. a., and Hermeking, H. (2005) The crystal structure of the non-liganded 14-3-3σ protein: Insights into determinants of isoform

specific ligand binding and dimerization. *Cell Res.* **15**, 219–227

41. Wilkert, E. W., Grant, R. A., Artim, S. C., and Yaffe, M. B. (2005) A structural basis for 14-3-3σ functional specificity. *J. Biol. Chem.* **280**, 18891–18898

42. Petta, I., Dejager, L., Ballegeer, M., Lievens, S., Tavernier, J., De Bosscher, K., and Libert, C. (2016) The Interactome of the Glucocorticoid Receptor and Its Influence on the Actions of Glucocorticoids in Combatting Inflammatory and Infectious Diseases. *Microbiol. Mol. Biol. Rev.* **80**, 495–522

43. Nixon, M., Andrew, R., and Chapman, K. E. (2013) It takes two to tango: Dimerisation of glucocorticoid receptor and its anti-inflammatory functions. *Steroids.* **78**, 59–68

44. Perez-Riverol, Y., Csordas, A., Bai, J., Bernal-Llinares, M., Hewapathirana, S., Kundu, D. J., Inuganti, A., Griss, J., Mayer, G., Eisenacher, M., Pérez, E., Uszkoreit, J., Pfeuffer, J., Sachsenberg, T., Yilmaz, Ş., Tiwary, S., Cox, J., Audain, E., Walzer, M., Jarnuczak, A. F., Ternent, T., Brazma, A., and Vizcaíno, J. A. (2019) The PRIDE database and related tools and resources in 2019: Improving support for quantification data. *Nucleic Acids Res.* **47**, D442–D450

Abbreviations and nomenclature

CaIA: Calyculin A

Co-IP: Co-immunoprecipitation

DIG: Digoxigenin

DIPEA: N,N-Diisopropylethylamine

DMEM: Dulbecco's Modified Eagle Medium

DPBS: Dulbecco's Phosphate-Buffered Saline

EDT: 1,2-ethanedithiol

ERα: Estrogen receptor α

ERRγ: Estrogen-related receptor γ

FITC: fluorescein isothiocyanate

FP: Fluorescence polarization assay

FSK: Forskolin

GR: Glucocorticoid receptor

HATU: 1-[bis(dimethylamino)methylene]-1H-1,2,3-triazolo[4,5-b]pyridinium 3-oxid hexafluorophosphate

HR: Hinge region

LBD: Ligand binding domain

MINK1: Misshapen-like kinase 1

NMP: N-Methyl-2-pyrrolidone

NTD: N-terminal domain

PDA: Photodiode array

PDB: Protein Data Bank

PKA: Protein kinase A

PXR: Pregnane X receptor

ROCK1: Rho-associated protein kinase1

RP: Reverse phase

SPPS: solid-phase peptide synthesis

SPR: Surface plasmon resonance

TIS: Triisopropylsilane

Tables

Table 1. Binding affinity of mutated GR_pT524-pS617

Peptide name	Amino acid sequence	Binding affinity with 14-3-3ζ by FP	
		K_d (µM)	pK_d
GR_pT524-pS617	K T I V P A **pT** L P Q L T P G G G G G R S Y R Q S **pS** A N L L C F	0.018 ± 0.006	7.7
GR_K518A	**A** T I V P A **pT** L P Q L T P G G G G G R S Y R Q S **pS** A N L L C F	0.11 ± 0.03	7.0
GR_T524A-pS617	K T I V P A **A** L P Q L T P G G G G G R S Y R Q S **pS** A N L L C F	120 ± 3	3.9
GR_P526A	K T I V P A **pT** L **A** Q L T P G G G G G R S Y R Q S **pS** A N L L C F	1.2 ± 0.1	5.9
GR_R614A	K T I V P A **pT** L P Q L T P G G G G G R S Y **A** Q S **pS** A N L L C F	0.22 ± 0.02	6.7
GR_pT524-S617A	K T I V P A **pT** L P Q L T P G G G G G R S Y R Q S **A** A N L L C F	1.3 ± 0.3	5.9
GR_pS524-pS617	K T I V P A **pS** L P Q L T P G G G G G R S Y R Q S **pS** A N L L C F	0.14 ± 0.01	6.9

Binding affinity (K_d and pK_d) of GR_pT524-pS617, relevant peptides from the alanine scan and GR_pS524-pS617. The residues mutated into alanine are depicted in bold black and the phosphorylated sites in bold red. Measurements were performed as triplicates.

ed

Table 2. Data collection and refinement statistics (molecular replacement)

	Binary complex of 14-3-3ζ with human Glucocorticoid Receptor pT524 peptide	Binary complex of 14-3-3ζ with human Glucocorticoid Receptor pS617 peptide	Binary complex of 14-3-3ζ with human Glucocorticoid Receptor pT524 pS617 peptide
PDB entry	6YO8	6YMO	6YOS
Data collection			
Space group	C2	$P2_12_12_1$	$P4_32_12$
Cell dimensions			
a, b, c (Å)	158.65, 99.88, 84.81	72.28, 104.35, 112.43	60.21, 60.21, 284.21
α, β, γ (°)	90.00, 93.73, 90.00	90.00, 90.00, 90.00	90.00, 90.00, 90.00
Resolution (Å)	84.47-2.09 (2.12-2.09)	47.33-2.02 (2.02-2.07)	58.90-2.75 (2.90-2.75)
Rmerge	0.06	0.08	0.11
I / σI	9.0 (0.6)	12.07 (0.53)	12.4 (1.3)
Completeness (%)	98.3 (97.8)	99.6 (95.8)	98.3 (94.0)
Redundancy	3.4 (3.4)	6.5 (6.3)	9.4 (6.9)
Refinement			
Resolution (Å)	60.85-2.09	47.33-2.02	58.90-2.75
No. reflections	76,616	56,503	14,250
Rwork / Rfree	0.224 / 0.235	0.212 / 0.228	0.265 / 0.292
Clashscore	8	2	8
Ramachandran outliers (%)	0.2	0	0
Sidechain outliers (%)	4.0	2.0	5.8
RSRZ outliers (%)	6.0	7.9	7.4
Matthews coefficient ($Å^3$/dalton)	2.16	2.05	2.49
Solvent content (%)	43.08	39.99	50.60
No. atoms			
Protein	7,693	3,769	3,690

Ligand/ion	0	25	0
Water	240	236	0
B-factors (Å^2)			
Protein	76.7	78.2	92.8
Ligand/ion	-	59.5	-
Water	68.0	68.9	-
R.m.s. deviations			
Bond lengths (Å)	0.72	0.49	0.90
Bond angles (°)	0.69	0.60	0.86
Interface parameters			
Buried surface area (sq Å)	761.8 (46.1%)	525.8 (63.1%)	1,247.4 (43.3%)
Interface area (sq Å)	675.7	460.0	1,132.5
Delta G (kcal/mol)	-12.2	-3.9	-16.9
Binding energy (kcal/mol)	-18.0	-16.9	-27.7
P value	0.5042	0.5829	0.5381
Hydrogen bonds	13	11	24
Effect of crystal contacts	The closest crystallographic neighbor is over 4Å away and is therefore unlikely to effect the binding of GR_pT524	The closest crystallographic neighbor is over 4Å away and is therefore unlikely to effect the binding of GR_pS617	The closest crystallographic neighbor is over 4Å away and is therefore unlikely to effect the binding of GR_pT524-pS617

*Values in parentheses are for highest-resolution shell.

Table 3. Phosphorylation of GR LBD by five kinases identified from the kinase screen

Kinase name	Number of GR phosphorylation	GR phosphorylation sites with strong evidence	GR phosphorylation sites with weak evidence
MAP4K4	1 and 2	T519 and T562	
MINK1	1 and 2	T524 and T562	T635
MST1	Up to 5	T562, T668, S682 and S746	T524, T594 and T635
MST2	Up to 7	T562, T668, S682 and S746	T519, T556 and T635
ROCK1	1	T519 and S617	

For each kinase, intact mass and peptide mapping enable the identification of the phosphorylation state and phosphorylation sites. The kinases further investigated are highlighted in grey.

Figures and figure legends

A

B

Peptide name	Amino acid sequence	K_d with 14-3-3ζ by FP (µM)
GR_pS83	DLSKAV**pS**LSMGLY	72 ± 30
GR_pS134	NLNRST**pS**VPENPK	90 ± 38
GR_pT493	NLEARK**pT**KKKIKG	>150
GR_pT524	KTIVPA**pT**LPQLTP	38 ± 8
GR_pT561	STWRIM**pT**TLNMLG	77 ± 36
GR_pS617	RSYRQS**pS**ANLLCF	25 ± 4
GR_pT635	INEQRM**pT**LPCMYD	55 ± 19
GR_pT8	DSKESL**pT**PGREEN	>150
GR_pS45	VKVSAS**pS**PSLAVA	>150
GR_pS113	QGQISL**pS**SGETDL	>150
GR_pS203	LEFSSG**pS**PGKETN	>150
GR_pS211	GKETNE**pS**PWRSDL	>150
GR_pS226	DENCLL**pS**PLAGED	>150
GR_pS234	LAGEDD**pS**FLLEGN	>150
GR_pS267	GDLVLS**pS**PSNVTL	>150
GR_pS404	MRPDVS**pS**PPSSSS	>150

C

Peptide name	Amino acid sequence	K_d with 14-3-3ζ by SPR (µM)
GR_pT524	KTIVPA**pT**LPQLTP	22 ± 8
GR_pS617	RSYRQS**pS**ANLLCF	27 ± 8

D

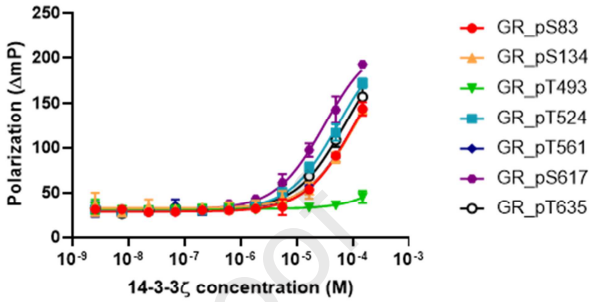

E

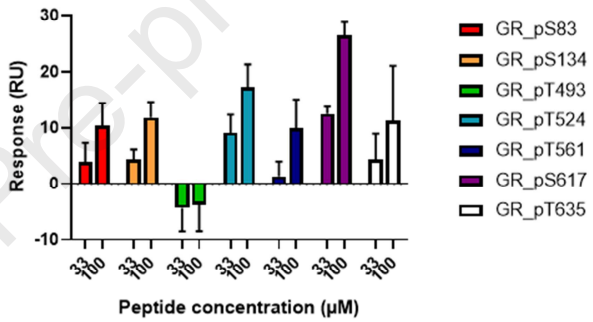

F

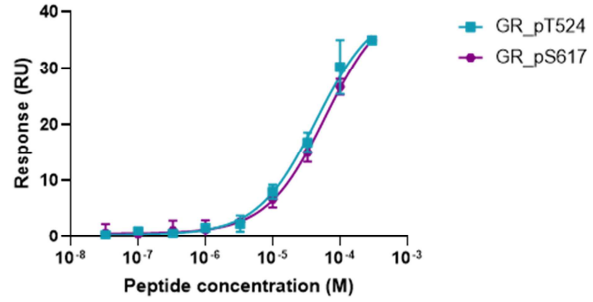

Fig. 1. Interaction of GR mono phosphopeptides with 14-3-3ζ. (**A**), Schematic representation of the GR sequence. The number of the residues located at the interface of each GR domain is reported below the sequence. (**B**), Amino acid sequences of the monophosphorylated GR peptides centered on the key residues and their binding affinity (K_d) measured by FP. Binding sites of GR from the literature are depicted in bold black and prediction in bold red. The most potent GR peptides are highlighted in grey. (**C**), K_d of the two most potent monophosphorylated GR peptides measured by SPR. (**D**), Concentration-response curves of FP assays of seven peptides centered on predicted 14-3-3 binding sites with 14-3-3ζ. (**E**), Affinity of monophosphorylated GR peptides with 14-3-3ζ measured by SPR at two different peptide concentrations (33 and 100 µM). (**F**), Concentration-response curves of SPR assays of the two most

potent peptides with 14-3-3ζ. All measurements were performed as triplicates and the error bars represent the standard deviation of these three independent experiments.

A

Peptide name	K_d with 14-3-3ζ by FP (μM)
GR_pT524-pS617	0.018 ± 0.006
GR_pS83-pT524	0.90 ± 0.1
GR_pS134-pT524	0.55 ± 0.1
GR_pS83-pS134	22 ± 8

B

Peptide name	K_d with 14-3-3ζ by SPR (μM)
GR_pT524-pS617	0.030 ± 0.024

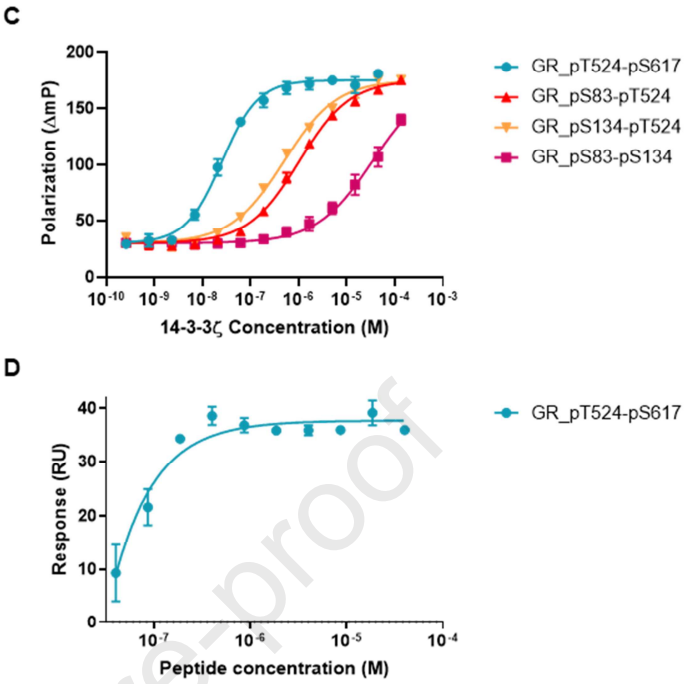

Fig. 2. Interaction of GR doubly phosphorylated peptides with 14-3-3ζ. (**A**), Binding affinity (K_d) of the diphosphorylated GR peptides measured by FP. The most potent GR peptide is highlighted in grey. (**B**), Binding affinity (K_d) of GR_pT524-pS617 measured by SPR. (**C**), Concentration-response curves of FP assays of the four diphosphorylated GR peptides with 14-3-3ζ. (**D**), Concentration-response curve of SPR assays of GR_pT524-pS617 with 14-3-3ζ. Measurements were performed as triplicates and the error bars represent the standard deviation of these three independent experiments.

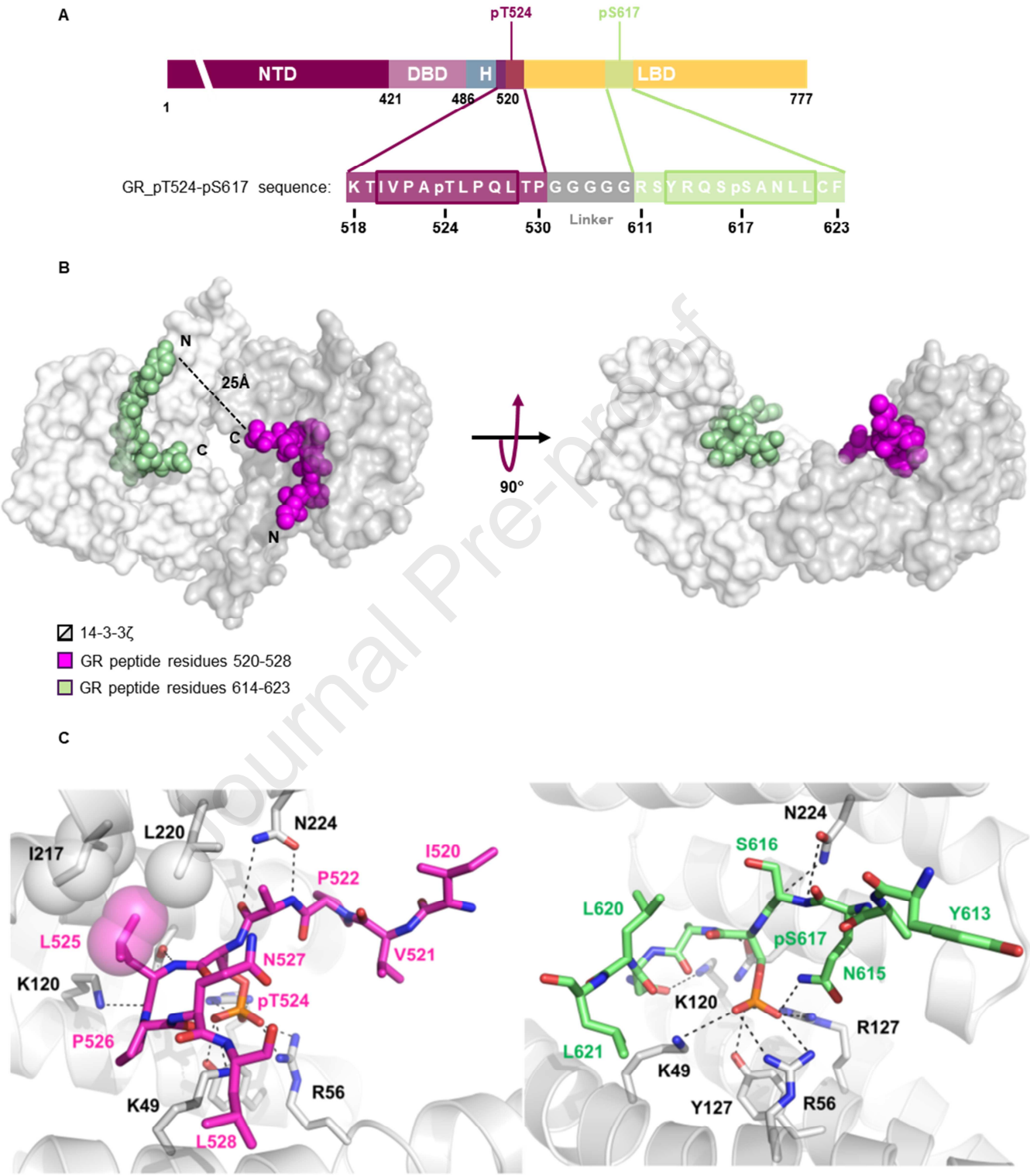

Fig. 3. Crystal structure of GR_pT524-pS617 bound to 14-3-3ζ dimer. (**A**), Location within the GR sequence of the two 13-mer peptides centered on pT524 and pS617 respectively, and sequence of

GR_pT524-pS617. The framed amino acids were assigned in the X-ray structure. (**B**), Surface representation of 14-3-3ζ dimer (white and grey solid surface) complexed with GR_pT524-pS617. Residues 520-528 are depicted in magenta and residues 614-623 in green. The black dashed line shows amino acid residues, not observed in the electron density, connecting the two binding sites. (**C**), Details of the interaction between GR_pT524-pS617 and 14-3-3ζ. Polar interactions are depicted as black dotted lines and hydrophobic contracts as magenta or white spheres with a semi-transparent surface.

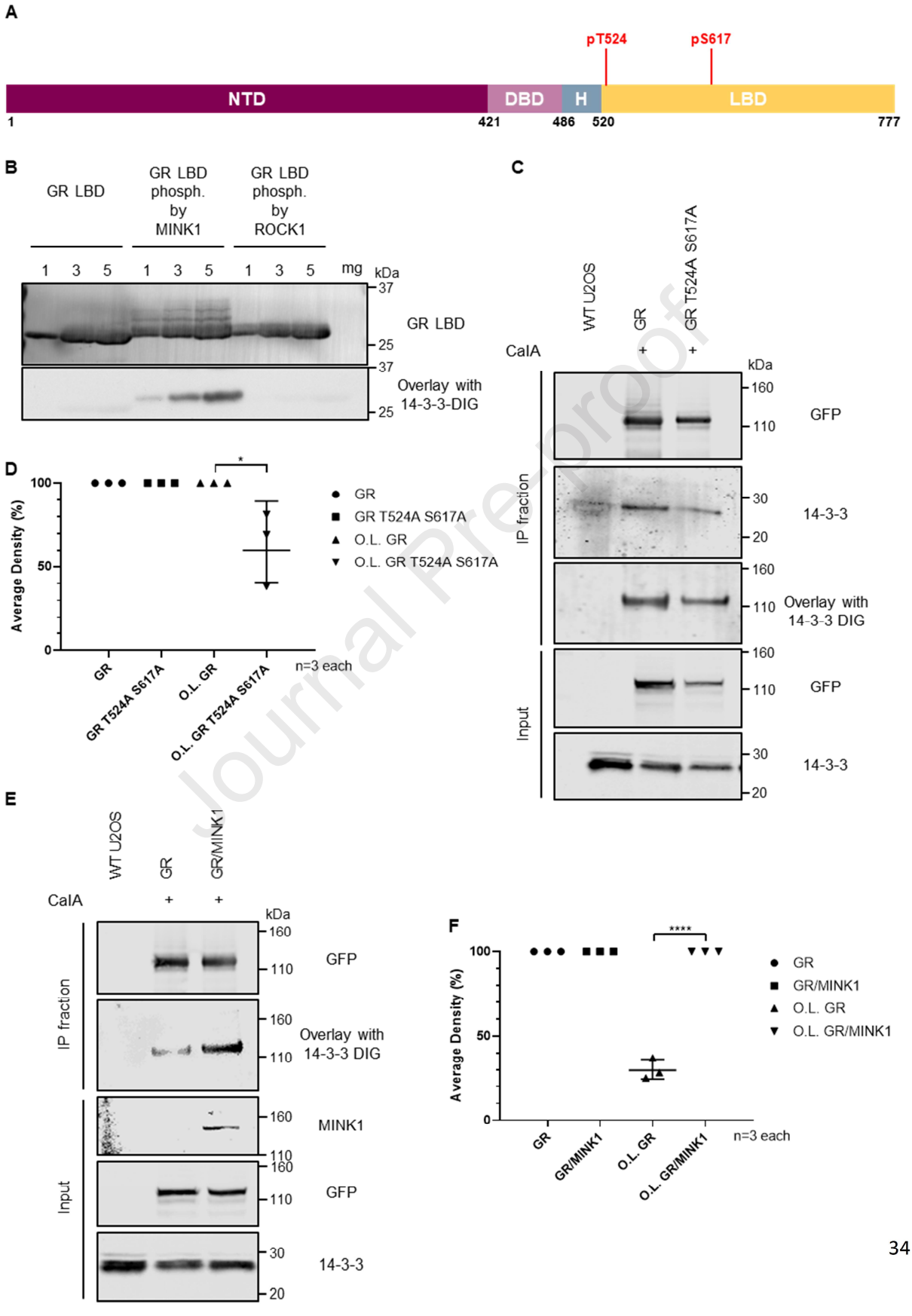

Fig. 4. Interaction of GR LBD and full length GR with pan 14-3-3. (**A**), Location within the GR sequence of pT524 and pS617. (**B**), Far-Western blotting overlay of GR LBD phosphorylated by MINK1 or ROCK1 with BMH1-BMH2-digoxygenin. Unphosphorylated and *in vitro* phosphorylated GR LBD were detected using anti-6X His tag antibody. GR LBD-bound 14-3-3 proteins were detected using anti-DIG antibody. (**C**), U2OS cells were transfected with GFP-GR or GFP-GR T524A S617A plasmids, and stimulated with calyculin A. Cell lysates were immunoprecipitated with GFP-Trap beads. GFP-GR and GFP-GR mutant were detected using anti-GFP antibody, GR-associated 14-3-3 was detected using anti-pan 14-3-3 antibody. Far-Western blotting overlay was done by incubation of the GR-containing membrane with BMH1-BMH2-DIG and subsequent detection of GR-bound 14-3-3 protein using anti-DIG antibody. (**D**), Quantification of three independent experiments. (**E**), U2OS cells were transfected with GFP-GR or cotransfected with GFP-GR and FLAG-MINK1 plasmids, and treated as previously mentioned. FLAG-MINK1 was detected using anti-MINK1 antibody. Far-Western blotting overlay was done as previously mentioned. (**F**), Quantification of three independent experiments. Data is normalized to the amount of GFP-GR and GFP-GR mutant from the IP fraction. The error bars represent the standard deviation of the three independent assays. O.L=overlay, CaIA=calyculin A. All p values were obtained using t-test. *$p < 0.05$, ****$p < 0.0001$.

A

B

Peptide name	Amino acid sequence	K_d with 14-3-3ζ by FP (μM)
GR_pS83	D L S K A V **pS** L S M G L Y	72 ± 30
GR_pS134	N L N R S T **pS** V P E N P K	90 ± 38
GR_pT493	N L E A R K **pT** K K K I K G	>150
GR_pT524	K T I V P A **pT** L P Q L T P	38 ± 8
GR_pT561	S T W R I M **pT** T L N M L G	77 ± 36
GR_pS617	R S Y R Q S **pS** A N L L C F	25 ± 4
GR_pT635	I N E Q R M **pT** L P C M Y D	55 ± 19
GR_pT8	D S K E S L **pT** P G R E E N	>150
GR_pS45	V K V S A S **pS** P S L A V A	>150
GR_pS113	Q G Q I S L **pS** S G E T D L	>150
GR_pS203	L E F S S G **pS** P G K E T N	>150
GR_pS211	G K E T N E **pS** P W R S D L	>150
GR_pS226	D E N C L L **pS** P L A G E D	>150
GR_pS234	L A G E D D **pS** F L L E G N	>150
GR_pS267	G D L V L S **pS** P S N V T L	>150
GR_pS404	M R P D V S **pS** P P S S S S	>150

C

Peptide name	Amino acid sequence	K_d with 14-3-3ζ by SPR (μM)
GR_pT524	K T I V P A **pT** L P Q L T P	22 ± 8
GR_pS617	R S Y R Q S **pS** A N L L C F	27 ± 8

D

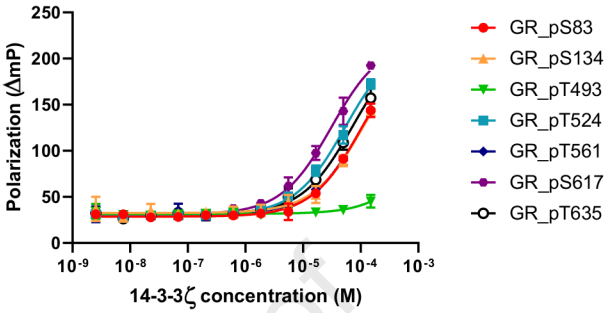

E

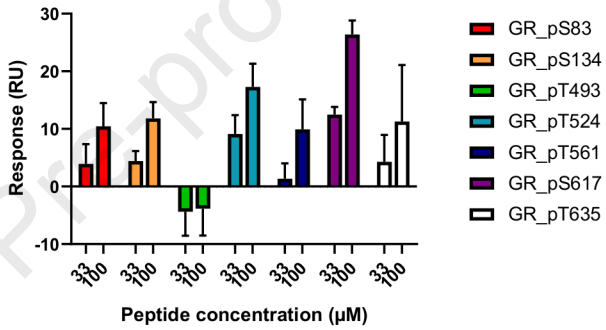

F

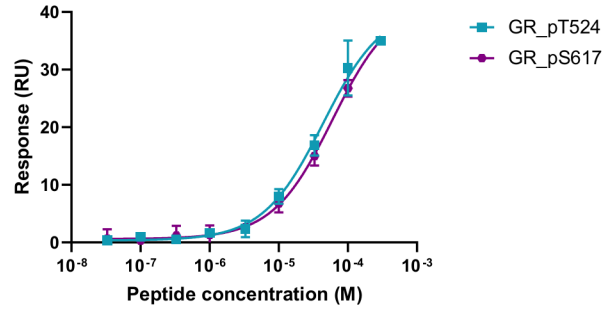

A

Peptide name	K_d with 14-3-3ζ by FP (μM)
GR_pT524-pS617	0.018 ± 0.006
GR_pS83-pT524	0.90 ± 0.1
GR_pS134-pT524	0.55 ± 0.1
GR_pS83-pS134	22 ± 8

B

Peptide name	K_d with 14-3-3ζ by SPR (μM)
GR_pT524-pS617	0.030 ± 0.024

C

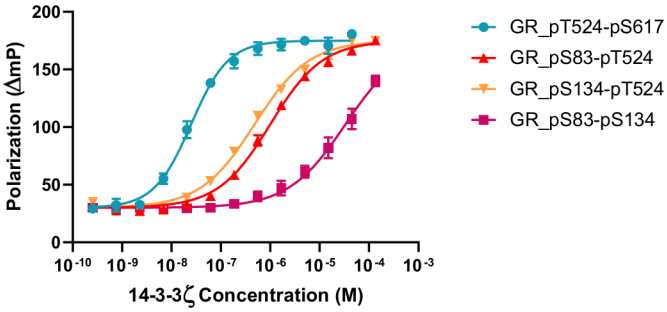

D

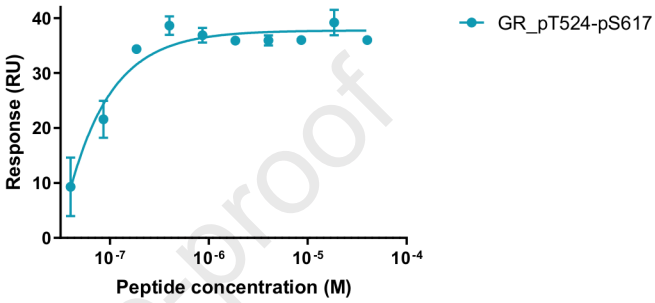

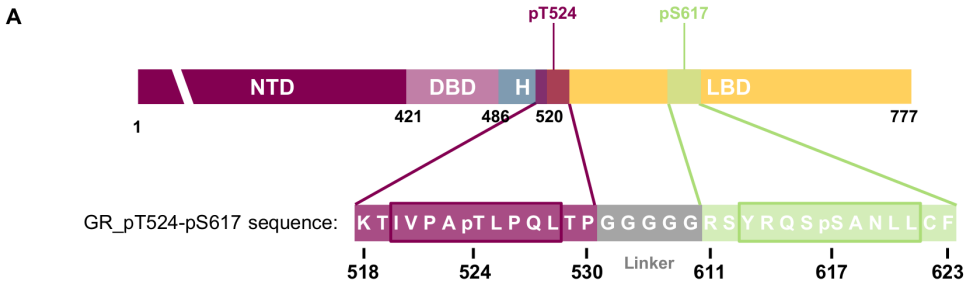
A
pT524
pS617
NTD
DBD
H
LBD
1
421
486
520
777
GR_pT524-pS617 sequence:
K T I V P A pT L P Q L T P G G G G G R S Y R Q S pS A N L L C F
518
524
530
Linker
611
617
623

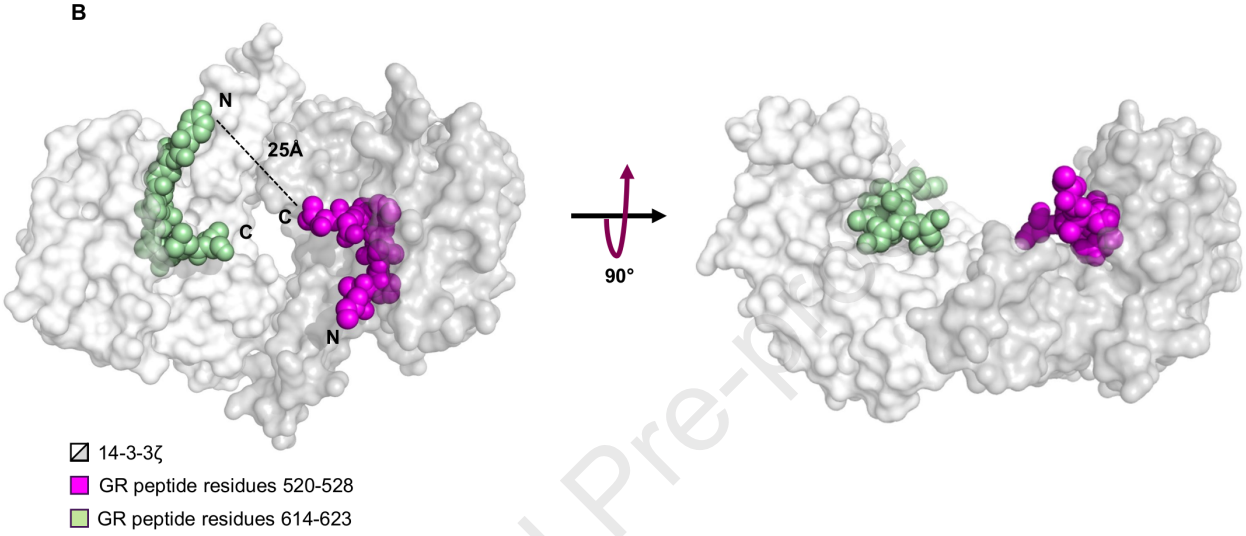
B
N
25Å
C
C
N
90°
14-3-3ζ
GR peptide residues 520-528
GR peptide residues 614-623

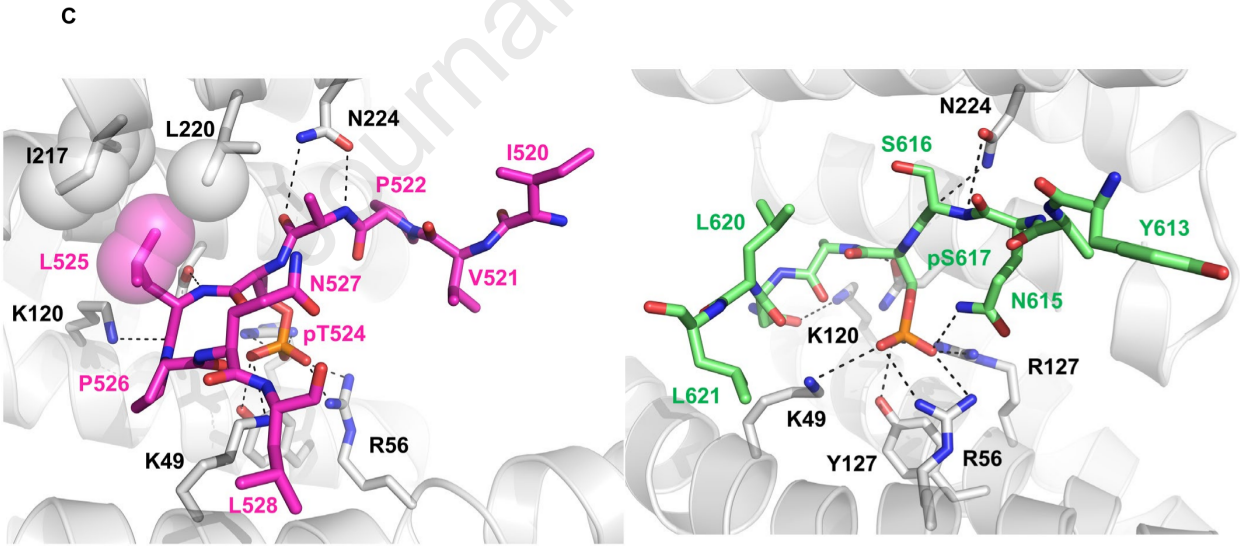
C
L220
N224
I217
I520
P522
L525
N527
V521
K120
pT524
P526
K49
R56
L528
N224
S616
L620
Y613
pS617
N615
K120
R127
L621
K49
Y127
R56